

N^2C : Neural Network Controller Design Using Behavioral Cloning

Shoaib Azam, *Student Member, IEEE*, Farzeen Munir, *Student Member, IEEE*,
Muhammad Aasim Rafique, *Member, IEEE*, Ahmad Muqem Sheri, *Member, IEEE*, Muhammad Ishfaq
Hussain, *Student Member, IEEE*, and Moongu Jeon, *Senior Member, IEEE*,

Abstract—Modern vehicles communicate data to and from sensors, actuators, and electronic control units (ECUs) using Controller Area Network (CAN) bus, which operates on differential signaling. An autonomous ECU responsible for the execution of decision commands to an autonomous vehicle is developed by assimilating the information from the CAN bus. The conventional way of parsing the decision commands is motion planning, which uses a path tracking algorithm to evaluate the decision commands. This study focuses on designing a robust controller using behavioral cloning and motion planning of autonomous vehicle using a deep learning framework. In the first part of this study, we explore the pipeline of parsing decision commands from the path tracking algorithm to the controller and proposed a neural network-based controller (N^2C) using behavioral cloning. The proposed network predicts throttle, brake, and torque when trained with the manual driving data acquired from the CAN bus. The efficacy of the proposed method is demonstrated by comparing the accuracy with the Proportional-Derivative-Integral (PID) controller in conjunction with the path tracking algorithm (pure pursuit and model predictive control based path follower). The second part of this study complements N^2C , in which an end-to-end neural network for predicting the speed and steering angle is proposed with image data as an input. The performance of the proposed frameworks are evaluated in real-time and on the Udacity dataset, showing better metric scores in the former and reliable prediction in the later case when compared with the state-of-the-art methods.

Index Terms—Autonomous vehicle control, Behavioral Cloning, Long short-term memory, Controller Area Network (CAN).

I. INTRODUCTION

Autonomous driving is one of the most computation extensive areas of the automobile industry and demands the development of new techniques utilizing mature sensors suite. The automation level in an autonomous vehicle is introduced by the Society of Automation Engineering (SAE) where, level-0 is manual control, and level-5 corresponds to fully autonomous mode¹. Besides, an increase in the automation level, safety of the autonomous vehicle in a dynamic traffic environment is a primary concern of many stakeholders,

Shoaib Azam, Farzeen Munir, Muhammad Ishfaq Hussain, and Moongu Jeon are with the School of Electrical Engineering and Computer Science, Gwangju Institute of Science and Technology, Gwangju, South Korea.

Muhammad Aasim Rafique and Ahmed Muqem Sheri are with National University of Sciences and Technology (NUST), Islamabad, Pakistan. e-mail: (shoibazam@gist.ac.kr; farzeen.munir@gist.ac.kr; ishfaqhussain@gist.ac.kr; aasim.rafique@seecs.edu.pk; muqem@mcs.edu.pk; mgjeon@gist.ac.kr)

¹<https://www.sae.org/news/2019/01/sae-updates-j3016-automated-driving-graphic>



Fig. 1: Our autonomous vehicle is equipped with state-of-the-art sensors.

including academicians, industrialists, researchers, and policymakers. Engineers and researchers are striving to enhance the safety level. The safety measures as standardized by SOTIF-ISO/PAS-21448 (Safety of the intended functionality) incorporate both the hardware and software aspects of the autonomous vehicle to provide complete situational awareness without system failure².

An accurately assessed response (planning) and a precise execution (control) of the response is a desiderata of safety in autonomous vehicles. Besides external sensors, modern vehicles are equipped with many in-built sensors and electronic control units (ECUs) that provide extensive and real-time information about the car for the driver's safety and control. This massive amount of data is available by the Controller-Area-Network (CAN) bus developed by Robert Bosch in 1986 [1] that serves as a communication channel between different electronic components of the car. The longitudinal and lateral control of the autonomous vehicle maps the planned desired actions to the vehicle actuators through the CAN bus.

A complete framework of autonomous vehicle includes localization, perception, and planning modules. Localization enables an autonomous vehicle to localize itself in a dynamic environment. The two essential entities required for localization are 3D maps (offline or online) and map-matching algorithms. The localization of the autonomous vehicle is done using Normal Distribution Transform matching [2].

The perception module incorporates the classification of objects in the environment through commonly used sensor

²<https://www.daimler.com/innovation/case/autonomous/safety-first-for-automated-driving-2.htm>

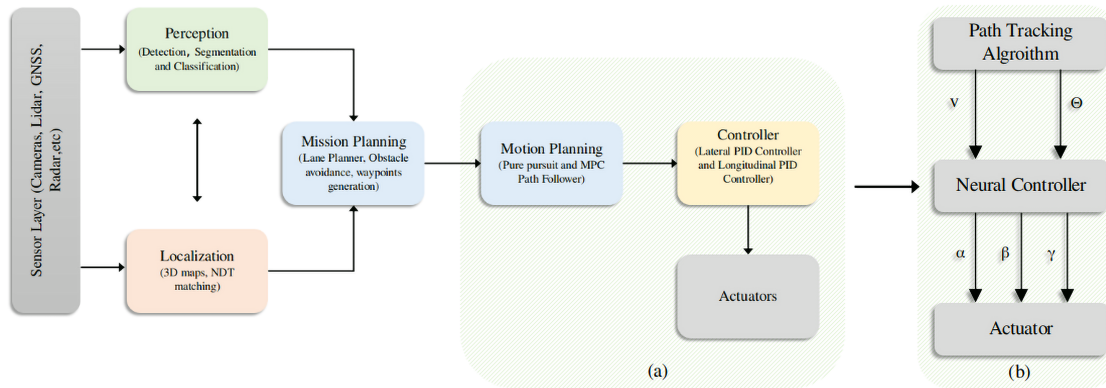


Fig. 2: The overall architecture of the autonomous vehicle is shown in this figure. (a) The conventional pipeline from motion planning to actuators using classical controllers [3]. (b) The proposed framework for designing a neural network-based controller. v and θ are linear and angular velocities from the path tracking algorithm. α , β , and γ are predicted throttle, brake, and torque from the neural network-based controller.

modalities that are lidar and camera. In the perception module, object detection, classification, and segmentation are done using lidar and image data. Yolo [4] and SSD [5] are used to perform image-based object detection, whereas euclidean clustering is used for lidar based object detection. SegNet is used for segmenting images [6], and PointPillars is used for segmentation and classification using lidar data [7]. The perception of an environment provides the necessary information about the environment, which is used by the planning module for motion and mission planning. In mission planning, a lane planner is devised by defining a state machine that tackles the object avoidance by incorporating the information from perception module. The mission planning generates the optimal waypoints used by the motion planning modules, including path tracking algorithms. Finally, the path tracking algorithm provides the desired linear and angular velocities information to the controller.

The control module plays an important role in predicting the behavior of an autonomous vehicle. There are two main categories of vehicle control i) longitudinal control, and ii) lateral control. The vehicle longitudinal control deals with vehicle speed regulation, and the lateral control is responsible for the sideways movement. In other words, vehicle speed and brake are managed by longitudinal control, whereas the steering angle is controlled by lateral control. The longitudinal and lateral control commands are transmitted to vehicle actuators through the CAN bus in terms of forces that includes throttle, brake, and torque. Generally, two separate controllers are utilized for controlling the autonomous vehicle. In literature, researchers have used different control strategies that include a Proportional-Integral-Derivative (PID) controller [8], predictive control mechanisms [9], and model-reference adaptive control methods [10].

The control and planning modules are associated in the stack of an autonomous vehicle using a path tracking algorithm. The planning module formulates an optimized path based on poses and velocities using mission and motion planning. A path tracking algorithm computes the linear and angular

velocity, which is fed to the controller for longitudinal and lateral movements. In this study, we explore the pipeline from the path-tracking algorithm to the controller, which includes i) path-tracking algorithm ii) longitudinal controller and iii) lateral controller using behavioral cloning. Fig. 2(b) shows a layout of the proposed framework. This study divides the proposed framework into two parts for ease of understanding, where the first part focuses on the design of a neural network-based controller (N^2C) using behavioral cloning [11] [12]. The second part uses image data for the prediction of speed and steering angle and a deep learning surrogates path tracking algorithm. For the neural network-based controller (N^2C) using behavioral cloning, the human driving data is collected that includes throttle (drive pedal), brake (brake pedal), torque (steering torque), speed and steering angle through CAN bus along with corresponding image data.

Recent research has introduced an end-to-end deep neural network to predict the steering angle and speed from images. However, the values of steering angle and speed predicted by the deep neural network cannot be verified with a real-time experiment. For instance, the steering angle predicted by the network is not in the limits of actuator [13]. In the second part of this work, we explore a strategy to verify the predictions of end-to-end deep neural network by predicting the steering angle and speed using images and feeding it to a neural network-based controller (N^2C), which in return generates throttle, brake, and torque for the vehicle actuators.

A. Background and Motivation

To develop a testbed for the autonomous vehicle, we modify an electric KIA Soul EV car. Fig. 1 shows our autonomous vehicle testbed equipped with perception and navigational sensors. In the perception sensors, lidar and cameras have been used for acquiring data for the perception of the environment. The location data is acquired using navigation sensors, which include a Global Navigation Satellite System (GNSS). It is an enclosed device containing the Global positioning System (GPS) and Inertial Measurement Unit (IMU). The GPS gives

the location with a tolerance of $2cm$ [14]. Fig. 2 shows the architecture of our autonomous vehicle.

The primary motivation of this work is to conduct an empirical study of replacement of the current modules of control architecture by neural network based on behavioral cloning. The experimental evaluation illustrates its advantages in terms of smoothness and robustness, for using N^2C and conventional control methods in juxtaposition. Second, this neural network-based controller model does not require human supervision for manual tuning of parameters as compared to conventional classical control theory.

The main contributions are listed as follows:

- 1) A novel controller is designed based on behavioral cloning using a neural network.
- 2) The designed neural network controller is utilized with the end-to-end approach of predicting steering angle and speed.
- 3) We have utilized the designed neural network-based controller (N^2C) with two different path-tracking algorithms to assess the efficacy of the proposed controller compared to the conventional classical controller.

The rest of the paper is organized as follows: Section II gives related work. Section III focuses on the proposed methodology. The experimentation and results are discussed in Section IV, and section V concludes the paper.

II. RELATED WORK

A. Control for autonomous vehicle

The control module of the autonomous vehicle is responsible for communicating with car electronics through CAN bus Fig. 2. It sends appropriate commands of the throttle, brake, and steering torque based on the angle and speed determine by the planning module to ECU [15]. In literature, the conventional control modules consist of longitudinal and lateral controllers that enable the autonomous vehicle to follow a planned trajectory [16]. These longitudinal and lateral controllers are designed using conventional approaches such as PID control [8], Linear-Quadratic Regulator control [9], Model predictive control [10], fuzzy logic [17], and so on. In recent years, the researchers are experimenting with classical control approaches with intelligent parameters tuning. [18] has proposed a fuzzy self-tuning PID controller for an autonomous vehicle. They have adopted a fuzzy logic on the top of the PID controller to address the problem of frequent switching between throttle and brake and also for optimizing the PID parameters online for nonlinear systems. [19] has used the artificial neural network to tune the PID parameters. [20] has combined the feed-forward PID controller with self-adapting PID to improve the accuracy of the control algorithm.

Model Predictive Control (MPC) or receding horizon control optimizes the control process by satisfying the constraints induced by the system dynamics model. MPC predicts the change in the future values in an iterative manner, by optimizing the cost function over the receding horizon. [21] has proposed the MPC based controller for steer and brake paddle control of an autonomous vehicle. They perform two formulations of the system, first tenth-order vehicle model,

and second simplified bicycle model. [22] has formulated an approach that combines the lane detection and model predictive control for accurate and stable control of the autonomous vehicle. The vehicle dynamics model consists of three degrees of freedom, and the fuzzy controller corrects the wheel steering angle. [23] introduces model predictive control higher-level controller in combination with a low-level controller generating steering wheel angle and drive pedal position for the autonomous vehicle. [24] introduces the Lyapunov-based approach with a Linear-Quadratic Regulator-Linear Matrix Inequality (LQR-LMI) tuning for control of the autonomous vehicle. The vehicle is modeled as a kinematic bicycle model. The nonlinear Lyapunov controller's parameters are optimized using a closed-loop system in linear parameter varying (LPV) form.

An autonomous vehicle (Sandstrom) uses a PID controller's variant as a feedback controller to regulate position and system actuators. They have used a simple geometric model for steering and speed control [25]. Stanley, the autonomous vehicle which won the DARPA challenge, develops a control layer that regulates the steering, brake, and throttle. Two closed-loop Proportional-Integral (PI) trajectory tracking controllers are developed, one for steering control and other for throttle and brake [26]. Boss has used model-predictive control to perform vehicle control [27]. Baidu Apollo uses a combination of three controllers, two low-level controllers consisting of feed-forward PID controller and LQR controller. A model-predictive controller is used as a higher-level controller to optimize PID and LQR parameters [28].

B. Prediction of steering angle and speed from images

In 1989, Pomerleau has made the first attempt to drive the car, Autonomous Land Vehicle in a Neural Network (ALVINN), using the information from images and laser finder [29]. (ALVINN) has demonstrated the autonomous steering of a vehicle on public roads. A simple neural network with 3 layers is trained in an end-to-end fashion, which shows the potential of ANN for autonomous navigation. Inspired by ALVINN, recently, a team of NVIDIA engineers has trained an end-to-end convolution neural network (CNN) that processes images from a front-facing camera [30]. The CNN learns the useful road features and predicts the steering commands. Du et al. explore two different frameworks to predict steering angle accurately and robustly using image data [31]. In the framework, the first network uses a 3D convolution layer combined with the LSTM unit's recurrent layers. The second network incorporates transfer learning to achieve high-quality results. Lu et al. have proposed an end-to-end neural model trained with temporal and spatial visual cues [32]. The framework is composed of the feature extracting sub-network and steering-prediction sub-network. The feature sub-network includes spatio-temporal convolution, multi-scale residual aggregation, and convolutional LSTM, followed by ReLU and dropout layers for extracting the features. The steering-prediction network includes LSTM for predicting the steering angle. Similarly, Chowdhuri et al. have used the behavior modalities and images to develop a multi-task and a

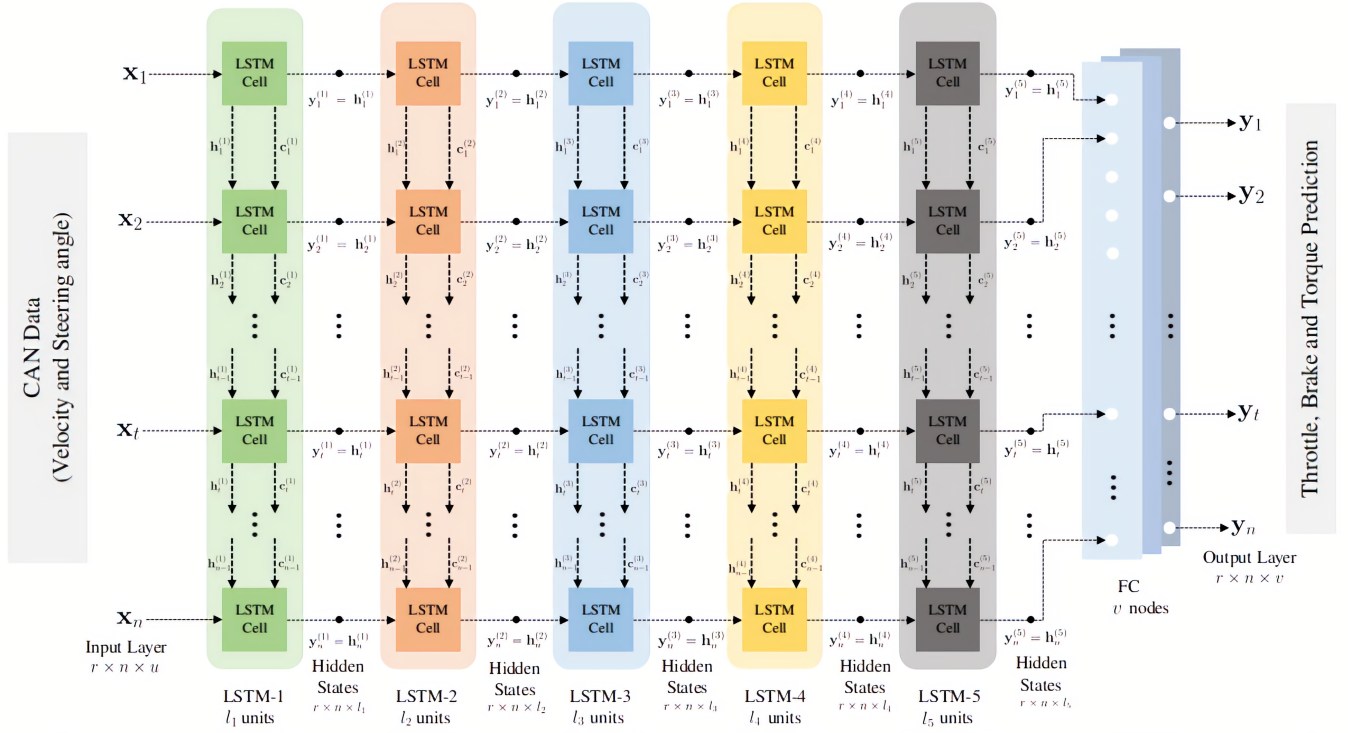


Fig. 3: The proposed framework for a controller, N^2C consisting of multi-layer LSTM architecture.

multi-model Z2Color network [33]. Yang et al. have predicted the steering angle and speed control using a multi-modal framework, which took information from previous speed and visual data [34].

Kim et al. have proposed a two-stage network [35]. The first stage consists of an end-to-end network that predicts the steering angle from images, and the second stage generates attention heat map from images, which emphasizes on the regions in the images that influence the output of the network. Xu et al. have introduced a novel FCN-LSTM network that jointly learns from steering and segmentation loss [36]. Hou et al. have proposed the FM-Net for the prediction of steering angle by incorporating the heterogeneous auxiliary networks for learning the steering angle [37]. In their work, they have used PSPNet [38] and Flownet [39] as an auxiliary network that provides the feature maps at three different levels; low, medium, and high for feature mimicking to train the network in an end-to-end manner for steering angle prediction.

III. PROPOSED METHOD

A. N^2C : Neural Network Controller Design

The neural network has been widely used as a function approximation for classification and regression problems. Besides the feed-forward neural network, recurrent neural network (RNNs) solves the sequence modeling problems by having recurrent connections between nodes of the network. RNNs with long short-term memory (LSTM) [40] units tend to capture sequential data dependencies, providing leverage to model the sequential structure of CAN bus data.

The standard deep LSTM architecture is the combination of input layers, LSTM layers, fully connected layers, and output

layers. In the LSTM layers, the basic building block is LSTM cells that map the input sequence layer to the output sequence layer. Fig. 5 shows the basic LSTM cell, which comprises of four interacting units: an internal cell, a forget gate, an input gate, and an output gate. The internal cell state at the previous time step is memorized at the internal cell through recurrent connections. The flow of input activation to the internal cell is controlled by the input cell. The forget gate is responsible for forgetting and resetting the cell memory adaptively, and an output layer controls the output activation flow to the LSTM cell. Suppose the input state to the LSTM cell is x_t , the input gate, forget gate, output gate, hidden state output and cell state memory are denoted by $i_t^l, f_t^l, o_t^l, h_t^l$ and c_t^l respectively at the time step t for l^{th} LSTM network layer. In addition, at time step $t - 1$ the hidden state output and cell memory state are represented by h_{t-1}^l and c_{t-1}^l respectively. The governing equation from Eq. (1)-Eq. (6) shows the relationship between the variables, as mentioned earlier.

$$i_t^l = \sigma(\mathbf{W}_{xi}^l \mathbf{x}_t + \mathbf{W}_{hi}^l \mathbf{h}_{t-1} + \mathbf{b}_i^l), \quad (1)$$

$$f_t^l = \sigma(\mathbf{W}_{xf}^l \mathbf{x}_t + \mathbf{W}_{hf}^l \mathbf{h}_{t-1} + \mathbf{b}_f^l), \quad (2)$$

$$o_t^l = \sigma(\mathbf{W}_{xo}^l \mathbf{x}_t + \mathbf{W}_{ho}^l \mathbf{h}_{t-1} + \mathbf{b}_o^l), \quad (3)$$

$$\tilde{c}_t^l = \tanh(\mathbf{W}_{xc}^l \mathbf{x}_t + \mathbf{W}_{hc}^l \mathbf{h}_{t-1} + \mathbf{b}_c^l), \quad (4)$$

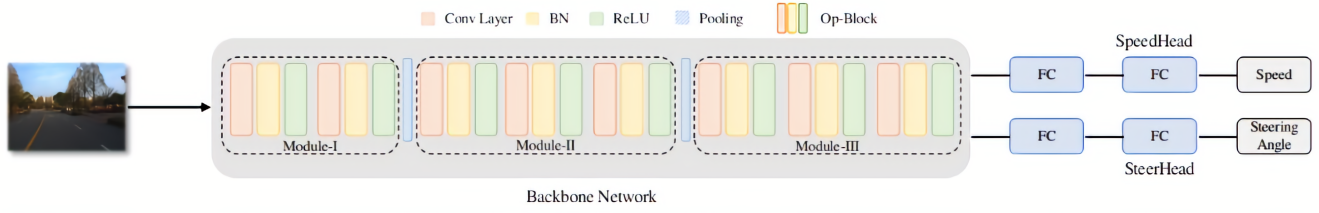


Fig. 4: The architecture for predicting steering angle and speed using image data. The architecture consists of a backbone network and the separate heads for both steering angle and speed prediction. The backbone network consists of three modules, followed by SpeedHead and SteerHead.

$$\mathbf{c}_t^l = \mathbf{f}_t^l \odot \mathbf{c}_{t-1}^l + \mathbf{i}_t^l \odot \tilde{\mathbf{c}}_t^l, \quad (5)$$

$$\mathbf{h}_t^l = \mathbf{o}_t^l \odot \tanh(\mathbf{c}_t^l), \quad (6)$$

where \mathbf{W} and \mathbf{b} represent the weight matrix and bias vector corresponding to different inputs within different gates.

In this study, a sequence to sequence LSTM network is used having multiple LSTM layers for the design of neural network based controller as illustrated in Fig. 3. It includes the input layer, five LSTM layers, one fully connected layer (FC), and the output layer. The number of units in the five LSTM layers are denoted by l_1, l_2, l_3, l_4 , and l_5 respectively. v represents the number of nodes in the FC layer. The input and output data for training the architecture is formatted in three dimensional where r shows the sample entries in the first dimension and n as a second dimension corresponds to time steps. The stack of five LSTM layers are used in the proposed network and based on that it is referred as $LSTM - 5$. Algorithm-1 illustrates the pseudo-code for the N^2C . The input to $LSTM - 5$ are linear velocity and steering angle. The input data is collected through behavioral cloning by driving the vehicle manually. The behavioral cloning is defined as learning from observations, in which the human observations are recorded along with actions. This human observation and action pairs are used by the learning agent to simulate the human behavior for that particular task. In this work, the human observations in term of throttle(drivepedal), brake (brakepedal) and torque along with linear velocity, and steering angle are recorded. The importance of using the behavioral

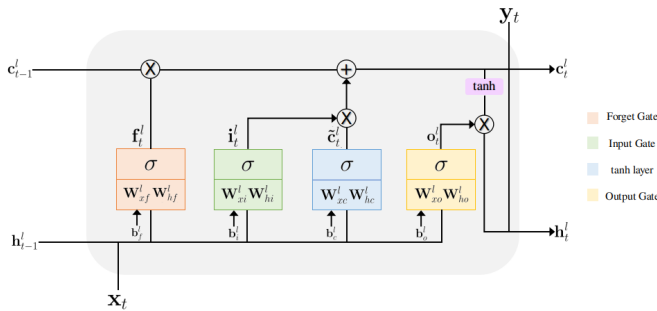


Fig. 5: The schematic of lstm cell which includes the input gate, output gate, forget gate and cell state memory.

cloning in this work, is to learn the human driving by observation and optimize the control of the autonomous vehicle through a learning algorithm in this case $LSTM - 5$ for smoothness of autonomous driving. The output of $LSTM - 5$ is a prediction of throttle, brake and torque. Let us denote the input to the $LSTM - 5$ as $\mathbf{X} = \mathbf{x}_1, \mathbf{x}_2, \mathbf{x}_3, \dots, \mathbf{x}_n^T \in \mathbb{R}^{n \times u}$ and output as $\mathbf{Y} = \mathbf{y}_1, \mathbf{y}_2, \mathbf{y}_3, \dots, \mathbf{y}_n^T \in \mathbb{R}^{n \times v}$ with n time steps. The input and output features are represented by u and v respectively. The rows in the both \mathbf{X} and \mathbf{Y} corresponds to time steps and the columns for features. The $LSTM - 5$ takes the input sequence \mathbf{X} and maps it for the prediction of output sequence \mathbf{Y} over the full duration of time steps ($t = 1, 2, 3, \dots, n$) with each LSTM cell in the LSTM layer is connected to its two neighbours ($t - 1, t, t + 1$). The network is trained by continually sending the \mathbf{x}_t to the $LSTM - 5$ over the entire temporal space using the repeated LSTM cells. At the end of the network, the fully connected layer (FC) is used to interlink the LSTM and target output layers in order to construct the desired output.

Algorithm 1: N^2C pseudo-code comprises of stacked LSTM layers.

Input: Linear Velocity and Steering Angle:

$$\mathbf{X} = \mathbf{x}_1, \mathbf{x}_2, \mathbf{x}_3, \dots, \mathbf{x}_n^T \in \mathbb{R}^{n \times u}$$

Result: Prediction of Throttle, Brake and Torque: \mathbf{Y}

Given parameters: $\mathbf{W}_{xi}, \mathbf{W}_{hi}, \mathbf{W}_{xf}, \mathbf{W}_{hf}, \mathbf{W}_{xo},$

$$\mathbf{W}_{ho}, \mathbf{W}_{xc}, \mathbf{W}_{hc}, \mathbf{b}_i, \mathbf{b}_f, \mathbf{b}_o, \mathbf{b}_c$$

Initialization of $\mathbf{h}_0, \mathbf{c}_0 = \mathbf{0}$

while $t \leq M$ do

Calculate \mathbf{i}_t using Eq. 1

Calculate \mathbf{f}_t using Eq. 2

Calculate $\tilde{\mathbf{c}}_t$ using Eq. 4

Update the cell state (\mathbf{c}_t) using Eq. 5

Calculate \mathbf{o}_t using Eq. 3

Calculate \mathbf{h}_t using Eq. 6

$\mathbf{t} \leftarrow \mathbf{t} + 1$

end

Output: $\mathbf{h} = [\mathbf{h}_1, \mathbf{h}_1, \dots, \mathbf{h}_n]$

$\mathbf{Y} = \tanh(\mathbf{h})$ Fully Connected layer

Result: Prediction of Throttle, Brake and Torque:

$$\mathbf{Y} = \mathbf{y}_1, \mathbf{y}_2, \mathbf{y}_3, \dots, \mathbf{y}_n^T \in \mathbb{R}^{n \times v}$$

B. End-to-End Prediction of Steering Angle and Speed

The second part of this study explores prediction of steering angle and speed using the images data with an end-to-end ANN, as shown in Fig. 4. A CNN is designed that takes image as input and predicts the steering angle and speed. The network is segregated into three parts i) backbone ii) SteerHead, and iii) SpeedHead. The backbone of the network extracts the features by passing the input image through a set of modules. In each module, a set of operations named op-block is performed on the input, which comprises convolution, batch normalization, and activation. A pooling layer is added after each module. In a particular module, the filter (K) size is increased by a factor of 2 whereas, the same kernel size F (3×3) is used. The encoded features from the backbone architecture are parsed to two fully connected heads, SpeedHead, and SteerHead, for the prediction of speed and steering angle, respectively.

IV. EXPERIMENTATION AND RESULTS

A. CAN Data Extractor

Real-time data is communicated between different electronic components in a vehicle through a standard CAN bus. In this study, a CAN bus data extractor is designed for the KIA Soul EV (our research testbed) that contains i) can-shield and ii) drivekit. The can-shield uses MCP2515 CAN bus controller with the SPI interface along with MCP2551 CAN transceiver. The can-shield provides the odometry data through the OBD-II CAN network at the speed of 1Mb/sec.

The drivekit³ serves as an electronic controller for the drive-by-wire vehicles that include the KIA Soul EV. The drivekit allows us to send and receive control commands through the OBD-II CAN network, which includes the vehicle's state information. The drivekit has its own CAN bus called Control CAN, which communicates with OBD-II CAN network through CAN Gateway. The communication through this mechanism ensures the safety of the vehicle's CAN bus.

Besides the hardware integration, the CAN messages are decoded using a can-sniffer⁴ algorithm in which the CAN arbitration identifiers are determined heuristically, by filtering out the specific arbitration identifiers corresponds to speed, steering angle, throttle, brake, and torque. The ROS node for can-shield and drivekit is used for extracting the data from both CAN data extractor mechanism.

B. Datasets

We used our research testbed with perceptual and navigational sensors for the data collection, as shown in Fig. 1. The perception sensor suite includes a 32 and 16 channels Velodyne lidar along with two FLIR BlackFly S cameras having a USB interface. Novatel GNSS is used as a navigational sensor for localization and mapping of the autonomous vehicle. The CAN data is extracted through drivekit and can-shield.

In our experimental study, only CAN bus and image data are collected. The CAN bus data includes throttle, brake, torque, speed, and steering angle, obtained through the vehicle

CAN bus using behavioral cloning while driving the vehicle manually. The throttle, brake values are normalized between $[0, 1]$ whereas, the torque values are between $[-1, 1]$. The speed values are recorded in m/s , and steering angle values are in radians. The CAN data is collected for two scenarios where one scene CAN data is used for training, and the other is used to test the proposed method. The training CAN data consists of 50,000 sequences, whereas the test CAN data consists of 17000 sequences. In recording the CAN bus data, there is no restriction of the speed limit, and the driver is free to drive the car in any manner, only by abiding the traffic rules. The image data is collected using our testbed that is composed of video frames. The image data and CAN bus data is synchronized and annotated with the respective steering angle and speed. In collecting the images data, the single front camera is used, having a resolution of 1440×1080 .

We have also used the Udacity⁵ dataset for the evaluation of the proposed method. The reason for using the Udacity dataset in contrast to other datasets, for instance, Comma.ai⁶, is that it includes CAN bus and image data which is advisable for our experimentation. In Comma.ai for instance, only image data with the corresponding steering angle is provided, and there is no speed information is available, irrespective of this, the Udacity dataset comprises of latitude, longitude, gear, brake, throttle, steering angles, speed, and image data.

C. N^2C Controller Design

This section focuses on implementing proposed $LSTM - 5$ architecture for the throttle, brake, and torque prediction, using human driving data of speed and steering angle. For the useful comparison of our proposed method, both the collected and Udacity datasets are used.

The training data consist of speed, steering angle, throttle, brake, and torque. The input to the network includes speed and steering angle whereas, throttle, brake, and torque serve as the output of the network. In the proposed method, both front and rear wheels speed are collected from the vehicle CAN bus. In training the neural network, all the wheel speed are averaged and used for the experimental evaluation. In order to train the $LSTM - 5$ network, both the input and output are converted into three-dimensional arrays. The first dimension entries correspond to samples, the second dimension represents the timestep, and the third dimension shows the input/output features/channels. Both input and output are fed to the $LSTM - 5$ for the training of the model after converting it to an input format. In addition, the training data is augmented with flipping, warping, and noise injection to enhance the trained network's generalization without being over-fitted to the train data. In training, the glorot uniform initializer is used for randomly initializing the weights of all LSTM layers and the FC layer, respectively. Besides, Adam (Adaptive Momentum Estimation) is used as an optimizer with a learning rate of 0.008, having a decay rate of 0.0001. The number of LSTM cells in the $LSTM - 5$ network layers are (300, 250, 100, 50, 20) and this configuration is chosen

³<https://github.com/PolySync/oscc>

⁴<https://github.com/linux-can/can-utils>

⁵<https://github.com/udacity/self-driving-car>

⁶<https://github.com/commaai/comma2k19>

TABLE I: RMSE and MAE scores of the proposed method using mse as loss function on the collected dataset.

Networks	Human Driving		PP+NN		PP+PID		MPC+NN		MPC+PID	
	RMSE	MAE	RMSE	MAE	RMSE	MAE	RMSE	MAE	RMSE	MAE
LSTM-5 Network	0.05593	0.032	0.0596	0.0429	0.1075	0.0664	0.057	0.0367	0.0802	0.0492
Conv-LSTM	0.0643	0.0381	0.0796	0.0477	0.1075	0.0664	0.065	0.0425	0.0802	0.0492
Conv	0.0683	0.0421	0.0958	0.0511	0.1075	0.0664	0.0697	0.0493	0.0802	0.0492

TABLE II: RMSE and MAE scores of the proposed method using smooth-L1 as loss function on the collected dataset.

Networks	Human Driving		PP+NN		PP+PID		MPC+NN		MPC+PID	
	RMSE	MAE	RMSE	MAE	RMSE	MAE	RMSE	MAE	RMSE	MAE
LSTM-5 Network	0.04963	0.03403	0.0547	0.0419	0.1075	0.0664	0.0515	0.0355	0.0802	0.0492
Conv-LSTM	0.0558	0.037	0.0789	0.0461	0.1075	0.0664	0.0598	0.0373	0.0802	0.0492
Conv	0.0624	0.04	0.0854	0.0491	0.1075	0.0664	0.0653	0.0402	0.0802	0.0492

empirically. The training process runs for a total of 500 epochs, with the batch size of 32 using the Keras and Tensorflow deep learning library on the Nvidia GTX 1080Ti GPU card. In our case, the two different loss function is used for the experimentation i) mean squared error (MSE) ii) Huber loss (smooth-L1 loss). The mean squared error (MSE) and Huber loss (smooth-L1 loss) are mathematically given by Eq. (7) and Eq. (8).

$$MSE = \frac{1}{k} \sum_{i=1}^k (y_k - \hat{y}_k)^2, \quad (7)$$

$$L_{\delta}(x) = \begin{cases} \frac{1}{2}x^2 & \text{for } |x| \leq \delta \\ \delta(|x| - \frac{1}{2}\delta) & \text{otherwise} \end{cases} \quad (8)$$

where in Huber loss, the value of $\delta = 1.0$ is used in experimentation.

1) *Analysis:* The proposed method’s effectiveness is determined by evaluating the trained model N^2C on the collected test data and Udacity data. It is also analyzed with a PID controller in combination with the path tracking algorithm. The path tracking algorithms used in the analysis are pure pursuit (PP) and model predictive control (MPC) based path follower. These path tracking algorithms are implemented and tested on testbed along with the PID controller. The angular velocity from the path tracking algorithm is converted to the steering angle before evaluation. For evaluation metric, root mean squared error (RMSE) and mean absolute error (MAE) are used. Table. I, and Table. II shows the evaluation results of N^2C with PID along with pure pursuit and mpc based path follower on the collected test dataset. The smaller RMSE and MAE values correspond to better accuracy. The RMSE and MAE scores are evaluated using both loss functions used in training the proposed model. RMSE and MAE are evaluated using the Eq. (9) and Eq. (10), respectively.

In Table. I, and Table. II, the human driving (proposed method only evaluated on human driving data) RMSE and MAE scores are evaluated only with the collected test data without any path tracking algorithm. Also, the proposed method, when used with path tracking algorithms (i-e PP+NN and MPC+NN) have better RMSE and MAE scores as compared to the PID controller with path tracking algorithms (PP+PID and MPC+PID). Fig. 8 shows the individual throttle,

TABLE III: Quantitative evaluation of effect of noise on N^2C for collected and Udacity datasets.

Human Driving								
Collected Dataset					Udacity Dataset			
Loss Function	Smooth-L1		MSE		Smooth-L1		MSE	
Networks	RMSE	MAE	RMSE	MAE	RMSE	MAE	RMSE	MAE
LSTM-5 Network	0.0505	0.0351	0.0612	0.0332	0.0578	0.0382	0.0654	0.0367
Conv-LSTM	0.0617	0.0382	0.0664	0.0391	0.0632	0.0396	0.0778	0.04012
Conv	0.0637	0.0422	0.071	0.0453	0.0721	0.0479	0.081	0.0496

brake, and torque RMSE and MAE scores of the proposed method for both loss functions only for human driving using collected test data. The individual comparison of the throttle, brake, and torque from the proposed method and PID along with pure pursuit and mpc based path follower is represented in Fig. 9.

The proposed method is also evaluated using the Udacity dataset. Table-IV shows the RMSE and MAE scores for the Udacity dataset. In this analysis, we have not experimented with the effect of the path tracking algorithm because, in the Udacity dataset, there is no information about the linear and angular velocities from the path tracking algorithm.

The N^2C is designed by training the neural network on data acquired from the vehicle CAN bus. The environmental conditions does not play any role in the prediction of controller output. In addition, the traffic condition are incorporated in the perception and planning modules of our autonomous vehicle stack. In this work, we have explicitly presented the neural network-based controller for the autonomous vehicle using behavioral cloning to provide smoothness to the control of autonomous vehicle. In addition, the proposed N^2C can be adapted for the other vehicles by replacing the CAN data extractor with the required vehicle CAN data extractor module. The fine tuning based on the N^2C will also be deployed for any other vehicle.

2) *Effect of Noise on N^2C :* In this section, the neural network-based controller’s performance for the effect of noise in case of inaccurate input data is evaluated. For the evaluation of controller, a Gaussian noise models having mean($\mu = 0$), and sigma($\sigma = 1$) is utilized. The experimentation is performed on test data for both the collected and Udacity datasets. Table-III illustrates the RMSE and MAE scores for the effect of noise on the controller output.

$$RMSE = \sqrt{\frac{1}{k} \sum_{j=1}^k (y_k - \hat{y}_k)^2}, \quad (9)$$

$$MAE = \frac{1}{k} \sum_{j=1}^k \|y_k - \hat{y}_k\|, \quad (10)$$

TABLE IV: RMSE and MAE scores of LSTM-5, Conv-LSTM and Conv network with smooth-L1 and mse loss function on Udacity dataset.

Human Driving				
Loss Function	Smooth-L1		MSE	
Networks	RMSE	MAE	RMSE	MAE
LSTM-5 Network	0.05314	0.0315	0.06253	0.0356
Conv-LSTM	0.05834	0.0325	0.07153	0.0421
Conv	0.06647	0.0424	0.07541	0.0489

3) *Ablation Study*: The proposed model, N^2C , is analyzed with different adjacent configurations in designing the neural network controller based on behavioral cloning. The experimentation is performed with a convolution neural network. Two networks are designed, including a single convolution layer and a Conv-LSTM network with a 1D convolution layer. In the first network, the five 1D convolution layers are used with ReLU as an activation function. After every two layers, dropout layers are used to regularize the training to reduce the over-fitting. The last dense layer of the network uses a *tanh* activation function so that the output values are sampled in the range of $[-1, 1]$. For the Conv-LSTM network, 1D convolution is applied to input data and then passed to the LSTM network. The network configuration of this network includes two 1D convolution layers, followed by four LSTM layers. The dropout layers are used after convolution layers, to avoid the overfitting. The mse and smooth-L1 Loss functions are used for training both of the networks.

Both of the network configurations are evaluated on test data as well as on the Udacity dataset. Table. I-Table-IV show the RMSE and MAE scores of these configurations. Fig. 8 shows the evaluation results of configurations when applied to the human driving test data. The individual analysis of throttle, brake, and torque for both configurations with PID and the path tracking algorithm on collected test data are shown in Fig. 10 and Fig. 11 respectively.

TABLE V: Mean RMSE and MAE score for Speed and Steering angle prediction.

Human Driving		
Dataset	RMSE	MAE
Ours	0.03045	0.021
Udacity	0.03325	0.026

Fig. 8, Fig. 9, Fig. 10, and Fig. 11 are shown at the end of manuscript.

TABLE VI: Comparison of RMSE scores of steering angle and speed prediction. * indicates the MSE scores are given for these algorithms which are converted to RMSE for comparison with our method. † shows the models tested on Udacity dataset.

Model	RMSE (Steering Angle)	RMSE (Speed)
Zero† [32]	0.2077	-
Mean† [32]	0.2098	-
AlexNet† [32]	0.1299	-
PilotNet† [32]	0.1604	-
VGG-16† [32]	0.0948	-
(ST-Conv + ConvLSTM +LSTM)† [32]	0.0948	-
[41]	0.0677	0.99206
[42]*	0.3660	0.05477
[36]*	0.4012	0.0812
Ours (collected dataset)	0.0249	0.036
Ours (Udacity dataset)	0.0298	0.0387

D. End-to-End Prediction of Steering Angle and Speed

In this section, the experimental details of the proposed method for predicting the steering angle and speed are discussed using image data.

The proposed network is trained for both datasets and include weather conditions for instance (sunny, overcast, shadows). The training data in both datasets consists of the pair of images and speed and steering angle values. Before training the network, the input image is downsampled to 400×400 dimension for efficiency purposes. The mean and standard deviation normalization is used for the input images. Also, data augmentation is also applied to input data which are as follows:

- 1) Randomly change the brightness by a factor of 0.2.
- 2) Randomly change the rotation of the input image by 20 degrees and shear angle randomly by 0.15 degrees.
- 3) Randomly flip the input image horizontally

In training, Adam optimizer is used with a learning rate of 0.001 with a decay rate of 0.0001. The model is trained for 300 epochs having the batch size of 12. The mean squared error (MSE) is used as a loss criterion for both speed and steering angle, and the overall model loss is the summation of both speed loss and steering angle loss.

For the quantitative analysis, RMSE and MAE scores are calculated on test data of the collected dataset. The proposed network for predicting the steering angle and speed are also evaluated on the Udacity dataset. Table- V shows the quantitative results on our data as well as on the Udacity dataset. The proposed method is also compared with other state-of-the-art algorithms. Table-VI represents the RMSE score of the proposed method, along with other state-of-the-art algorithms. Fig. 6 and Fig. 7 shows the quantitative results of speed and steering angle prediction on our dataset as well as on the Udacity dataset, respectively.

E. End-to-End prediction of speed and Steering angle with N^2C

A unified framework that includes the prediction of steering angle and speed along with the neural network controller, N^2C , has experimented in this section. In this framework, the predicted speed and steering angle is passed to the N^2C to predict the throttle, brake, and torque. For the evaluation,

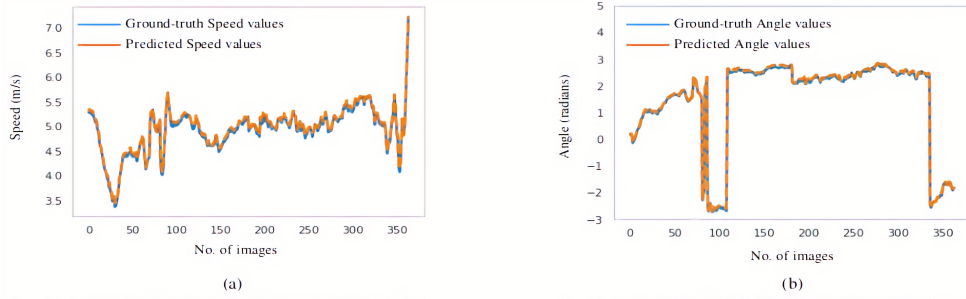


Fig. 6: Quantitative comparison between the ground-truth and predictive values for (a) speed, and (b) angle on the collected dataset.

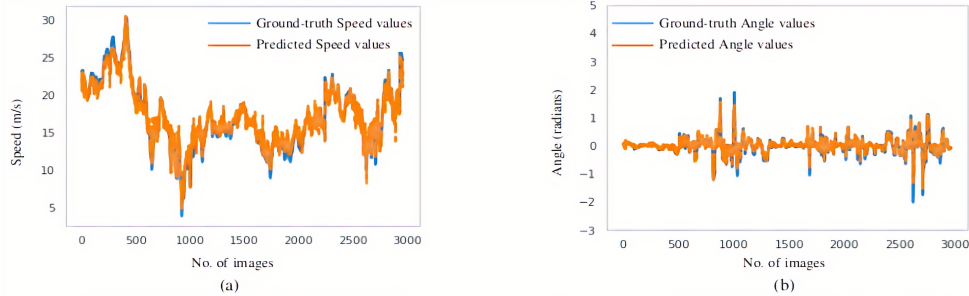


Fig. 7: Quantitative comparison between the ground-truth and predictive values for (a) speed, and (b) angle on Udacity dataset.

this architecture is tested on both datasets. Table-VII shows the RMSE and MAE scores. The effect of the loss function in N^2C is analyzed by computing the metric scores for both loss function, which are used in the design of N^2C .

V. CONCLUSION

In this paper, we proposed a controller (N^2C) for an autonomous vehicle constituted with an artificial neural network. The proposed controller (N^2C) is inspired by behavioral cloning, and prospects as a replacement of the classical control module in the autonomous vehicles. The designed neural network predicts throttle, brake, and torque by taking steering angle and speed as inputs. The experimental evaluation of the controller exhibits its usability in lieu of conventional classical controller when experimented with the two path tracking algorithms: pure pursuit and model predictive control based path follower. The evaluation results show better RMSE and MAE scores for N^2C in contrast to the conventional PID controller. The second part presented in this study is focused on the design of an end-to-end ANN that predicts steering angle and speed from images. The experimental results show the better metric scores of end-to-end ANN in predicting speed

and steering angle on the collected and Udacity datasets compared to state-of-the-art methods. Further, as a supplement, the N^2C is also tested with an end-to-end steering angle and speed prediction ANN in a unified framework. The simulation results, in terms of better metric scores, show the efficacy that the unified framework provides a competitive replacement for the conventional pipeline of motion planning and control. In the proposed work, the N^2C predicts the throttle, brake and torques by taking the average wheel speed and steering angle as input. The possible limitations of the proposed work is to include other source of obtaining the speed. The fusion of speed from GNSS (also gives the average speed) and wheel speed in order to enhance the current experimentation results is one possible future work. In addition, the incorporation of dynamics of vehicles by along the lines of proposed work is another future aspect of the proposed work. The future work also includes the curriculum learning of the proposed controller with the inclusion of more human behaviours in order to simulate the controller act like human driving rather than a computerized controller. In addition, the fusion of observations from human steering using electromyography sensors with CAN bus data for the controller design is also a future prospect of this work.

TABLE VII: RMSE and MAE scores of unified network with smooth-L1 and mse loss function on collected and Udacity datasets.

Loss function	Smooth L1		MSE	
	RMSE	MAE	RMSE	MAE
Collected	0.05136	0.03097	0.0567	0.035
Udacity	0.05741	0.0336	0.06874	0.043

ACKNOWLEDGMENTS

This work was partly supported by the ICT R&D program of MSIP/IITP (2014-0-00077, Development of global multi-target tracking and event prediction techniques based on real-time large-scale video analysis), Institute of Information and Communications Technology Planning and Evaluation (IITP) grant funded by the Korea government (MSIT)(No.2019-0-01842, Artificial Intelligence Graduate School Program

(GIST)), Ministry of Culture, Sports and Tourism (MCST), and Korea Creative Content Agency (KOCCA) in the Culture Technology (CT) Research & Development (R2020070004) Program 2020.

REFERENCES

- [1] U. Kiencke, S. Dais, and M. Litschel, "Automotive serial controller area network," *SAE transactions*, pp. 823–828, 1986.
- [2] F. Munir, S. Azam, A. M. Sheri, Y. Ko, and M. Jeon, "Where am i: Localization and 3d maps for autonomous vehicles." in *VEHITS*, 2019, pp. 452–457.
- [3] S. Azam, F. Munir, and M. Jeon, "Dynamic control system design for autonomous car." in *VEHITS*, 2020, pp. 456–463.
- [4] A. Farhadi and J. Redmon, "Yolov3: An incremental improvement," *Computer Vision and Pattern Recognition*, cite as, 2018.
- [5] W. Liu, D. Anguelov, D. Erhan, C. Szegedy, S. Reed, C.-Y. Fu, and A. C. Berg, "Ssd: Single shot multibox detector," in *European conference on computer vision*. Springer, 2016, pp. 21–37.
- [6] V. Badrinarayanan, A. Kendall, and R. Cipolla, "Segnet: A deep convolutional encoder-decoder architecture for image segmentation," *IEEE transactions on pattern analysis and machine intelligence*, vol. 39, no. 12, pp. 2481–2495, 2017.
- [7] A. H. Lang, S. Vora, H. Caesar, L. Zhou, J. Yang, and O. Beijbom, "Pointpillars: Fast encoders for object detection from point clouds," in *Proceedings of the IEEE Conference on Computer Vision and Pattern Recognition*, 2019, pp. 12 697–12 705.
- [8] J. Pérez, V. Milanés, and E. Onieva, "Cascade architecture for lateral control in autonomous vehicles," *IEEE Transactions on Intelligent Transportation Systems*, vol. 12, no. 1, pp. 73–82, 2011.
- [9] R. Cristi, F. A. Papoulias, and A. J. Healey, "Adaptive sliding mode control of autonomous underwater vehicles in the dive plane," *IEEE journal of Oceanic Engineering*, vol. 15, no. 3, pp. 152–160, 1990.
- [10] F. Borrelli, P. Falcone, T. Keviczky, J. Asgari, and D. Hrovat, "Mpc-based approach to active steering for autonomous vehicle systems," *International journal of vehicle autonomous systems*, vol. 3, no. 2-4, pp. 265–291, 2005.
- [11] F. Torabi, G. Warnell, and P. Stone, "Behavioral cloning from observation," *arXiv preprint arXiv:1805.01954*, 2018.
- [12] X. Zhang, M. Chen, and X. Zhan, "Behavioral cloning for driverless cars using transfer learning," in *2018 IEEE/ION Position, Location and Navigation Symposium (PLANS)*. IEEE, 2018, pp. 1069–1073.
- [13] T. Qiu and Z. Huang, "Learning a steering decision policy for end-to-end control of autonomous vehicle," in *2019 5th International Conference on Control, Automation and Robotics (ICCAR)*. IEEE, 2019, pp. 347–351.
- [14] F. Munir, S. Azam, M. I. Hussain, A. M. Sheri, and M. Jeon, "Autonomous vehicle: The architecture aspect of self driving car," in *Proceedings of the 2018 International Conference on Sensors, Signal and Image Processing*, 2018, pp. 1–5.
- [15] K. Kritayakirana and J. C. Gerdes, "Autonomous vehicle control at the limits of handling," *International Journal of Vehicle Autonomous Systems*, vol. 10, no. 4, pp. 271–296, 2012.
- [16] A. Khodayari, A. Ghaffari, S. Ameli, and J. Flahatgar, "A historical review on lateral and longitudinal control of autonomous vehicle motions," in *2010 International Conference on Mechanical and Electrical Technology*. IEEE, 2010, pp. 421–429.
- [17] K. Kodagoda, W. S. Wijesoma, and E. K. Teoh, "Fuzzy speed and steering control of an agv," *IEEE Transactions on control systems technology*, vol. 10, no. 1, pp. 112–120, 2002.
- [18] J. F. Wang and H. Zhao, "Speed control of tracked vehicle autonomous driving system using fuzzy self-tuning pid," in *2019 4th International Conference on Mechanical, Control and Computer Engineering (ICM-CCE)*. IEEE, 2019, pp. 305–3053.
- [19] X. Han, X. Zhang, Y. Du, and G. Cheng, "Design of autonomous vehicle controller based on bp-pid," in *IOP Conference Series: Earth and Environmental Science*, vol. 234, no. 1. IOP Publishing, 2019, p. 012097.
- [20] J. Wang, Y. Zhu, R. Qi, X. Zheng, and W. Li, "Adaptive pid control of multi-dof industrial robot based on neural network," *Journal of Ambient Intelligence and Humanized Computing*, pp. 1–12, 2020.
- [21] P. Falcone, H. Eric Tseng, F. Borrelli, J. Asgari, and D. Hrovat, "Mpc-based yaw and lateral stabilisation via active front steering and braking," *Vehicle System Dynamics*, vol. 46, no. S1, pp. 611–628, 2008.
- [22] J. Hu, S. Xiong, J. Zha, and C. Fu, "Lane detection and trajectory tracking control of autonomous vehicle based on model predictive control," *International journal of automotive technology*, vol. 21, no. 2, pp. 285–295, 2020.
- [23] G. Tosolin, J. Cartró, and V. Sharma, "Development of model predictive motion planning and control for autonomous vehicles," in *10th International Munich Chassis Symposium 2019*. Springer, 2020, pp. 323–340.
- [24] E. Alcalá, V. Puig, J. Quevedo, T. Escobet, and R. Comasolivas, "Autonomous vehicle control using a kinematic lyapunov-based technique with lqr-lmi tuning," *Control engineering practice*, vol. 73, pp. 1–12, 2018.
- [25] C. Urmson, C. Ragusa, D. Ray, J. Anhalt, D. Bartz, T. Galatali, A. Gutierrez, J. Johnston, S. Harbaugh, H. "Yu" Kato *et al.*, "A robust approach to high-speed navigation for unrehearsed desert terrain," *Journal of Field Robotics*, vol. 23, no. 8, pp. 467–508, 2006.
- [26] S. Thrun, M. Montemerlo, H. Dahlkamp, D. Stavens, A. Aron, J. Diebel, P. Fong, J. Gale, M. Halpenny, G. Hoffmann *et al.*, "Stanley: The robot that won the darpa grand challenge," *Journal of field Robotics*, vol. 23, no. 9, pp. 661–692, 2006.
- [27] C. Urmson, J. Anhalt, D. Bagnell, C. Baker, R. Bittner, M. Clark, J. Dolan, D. Duggins, T. Galatali, C. Geyer *et al.*, "Autonomous driving in urban environments: Boss and the urban challenge," *Journal of Field Robotics*, vol. 25, no. 8, pp. 425–466, 2008.
- [28] X. Huang, X. Cheng, Q. Geng, B. Cao, D. Zhou, P. Wang, Y. Lin, and R. Yang, "The apolloscape dataset for autonomous driving," in *Proceedings of the IEEE Conference on Computer Vision and Pattern Recognition Workshops*, 2018, pp. 954–960.
- [29] D. Pomerleau, "An autonomous land vehicle in a neural network. nips 1," 1989.
- [30] M. Bojarski, D. Del Testa, D. Dworakowski, B. Firner, B. Flepp, P. Goyal, L. D. Jackel, M. Monfort, U. Muller, J. Zhang *et al.*, "End to end learning for self-driving cars," *arXiv preprint arXiv:1604.07316*, 2016.
- [31] S. Du, H. Guo, and A. Simpson, "Self-driving car steering angle prediction based on image recognition," *arXiv preprint arXiv:1912.05440*, 2019.
- [32] L. Chi and Y. Mu, "Deep steering: Learning end-to-end driving model from spatial and temporal visual cues," *arXiv preprint arXiv:1708.03798*, 2017.
- [33] S. Chowdhuri, T. Pankaj, and K. Zipser, "Multinet: Multi-modal multi-task learning for autonomous driving," in *2019 IEEE Winter Conference on Applications of Computer Vision (WACV)*. IEEE, 2019, pp. 1496–1504.
- [34] Z. Yang, Y. Zhang, J. Yu, J. Cai, and J. Luo, "End-to-end multi-modal multi-task vehicle control for self-driving cars with visual perceptions," in *2018 24th International Conference on Pattern Recognition (ICPR)*. IEEE, 2018, pp. 2289–2294.
- [35] J. Kim and J. Canny, "Interpretable learning for self-driving cars by visualizing causal attention," in *Proceedings of the IEEE international conference on computer vision*, 2017, pp. 2942–2950.
- [36] H. Xu, Y. Gao, F. Yu, and T. Darrell, "End-to-end learning of driving models from large-scale video datasets," in *Proceedings of the IEEE conference on computer vision and pattern recognition*, 2017, pp. 2174–2182.
- [37] Y. Hou, Z. Ma, C. Liu, and C. C. Loy, "Learning to steer by mimicking features from heterogeneous auxiliary networks," in *Proceedings of the AAAI Conference on Artificial Intelligence*, vol. 33, 2019, pp. 8433–8440.
- [38] H. Zhao, J. Shi, X. Qi, X. Wang, and J. Jia, "Pyramid scene parsing network," in *Proceedings of the IEEE conference on computer vision and pattern recognition*, 2017, pp. 2881–2890.
- [39] E. Ilg, N. Mayer, T. Saikia, M. Keuper, A. Dosovitskiy, and T. Brox, "FlowNet 2.0: Evolution of optical flow estimation with deep networks," in *Proceedings of the IEEE conference on computer vision and pattern recognition*, 2017, pp. 2462–2470.
- [40] F. A. Gers, N. N. Schraudolph, and J. Schmidhuber, "Learning precise timing with lstm recurrent networks," *Journal of machine learning research*, vol. 3, no. Aug, pp. 115–143, 2002.
- [41] C. Zhao, J. Gong, C. Lu, G. Xiong, and W. Mei, "Speed and steering angle prediction for intelligent vehicles based on deep belief network," in *2017 IEEE 20th International Conference on Intelligent Transportation Systems (ITSC)*. IEEE, 2017, pp. 301–306.
- [42] S. Hecker, D. Dai, and L. Van Gool, "End-to-end learning of driving models with surround-view cameras and route planners," in *Proceedings of the european conference on computer vision (eccv)*, 2018, pp. 435–453.



Shoab Azam received a B.S. degree in Engineering Sciences from Ghulam Ishaq Khan Institute of Science and Technology, Pakistan, in 2010, and an M.S. degree in Robotics and Intelligent Machine Engineering from National University of Science and Technology, Pakistan, in 2015. He is currently pursuing a Ph.D. with the Department of Electrical Engineering and Computer Science, Gwangju Institute of Science and Technology, Gwangju, South Korea. His current research interests include deep learning and autonomous driving.



Farzeen Munir received the B.S. degree in Electrical Engineering from Pakistan Institute of Engineering and Applied Sciences, Pakistan in 2013, and MS degree in System Engineering from Pakistan Institute of Engineering and Applied Sciences, Pakistan in 2015. Now she is pursuing her PhD degree at Gwangju Institute of Science and Technology, Korea in Electrical Engineering and Computer Science. Her current research interest include, machine Learning, deep neural network, autonomous driving and computer vision.



Aasim Rafique received his M.Sc. degree in computer science from Quaid-e-Azam University, Islamabad, Pakistan. He then received his M.Sc. degree in computer science from Lahore University of Management and Sciences, Lahore, Pakistan in 2008. He received his Ph.D. degree from School of Electrical Engineering and Computer Sciences, GIST, Gwangju, Republic of Korea, in 2018. He is now working as Assistant Professor at School of Electrical Engineering and Computer Science, National University of Sciences and Technology (NUST), Pakistan. His research interests are artificial neural networks, their application in machine learning and computer vision.



Ahmad Muqem Sheri received the B.E. degree in computer software engineering from the National University of Science and Technology, Rawalpindi, Pakistan, and the M.S. degree in computer sciences from the Lahore University of Management and Sciences, Lahore, Pakistan, in 2008. He received his PhD degree in Computer Science from the School of Information and Communication, Gwangju Institute of Science and Technology, Gwangju, Korea. Currently he is working as an Assistant Professor in Department of Computer Software Engineering, National University of Sciences and Technology (NUST), Pakistan.



Muhammad Ishfaq Hussain received the B.Sc. degree from University of The Punjab Lahore, Pakistan in 2008, and M.S. degree in Computer Software Engineering from National University of Science and Technology, Pakistan in 2016. He is currently pursuing the Ph.D. degree with the Department of Electrical Engineering and Computer Science, Gwangju Institute of Science and Technology, Gwangju, South Korea. His current research interests include artificial intelligence and machine learning, sensor fusion, robotics, and autonomous driving.



Moongu Jeon received the B.S. degree in architectural engineering from Korea University, Seoul, South Korea, in 1988, and the M.S. and Ph.D. degrees in computer science and scientific computation from the University of Minnesota, Minneapolis, MN, USA, in 1999 and 2001, respectively. As a Post-Graduate Researcher, he worked on optimal control problems at the University of California at Santa Barbara, Santa Barbara, CA, USA, from 2001 to 2003, and then moved to the National Research Council of Canada, where he worked on the sparse representation of high-dimensional data and the image processing until 2005. In 2005, he joined the Gwangju Institute of Science and Technology, Gwangju, South Korea, where he is currently a Full Professor with the School of Electrical Engineering and Computer Science. His current research interests are in machine learning, computer vision, and artificial intelligence.

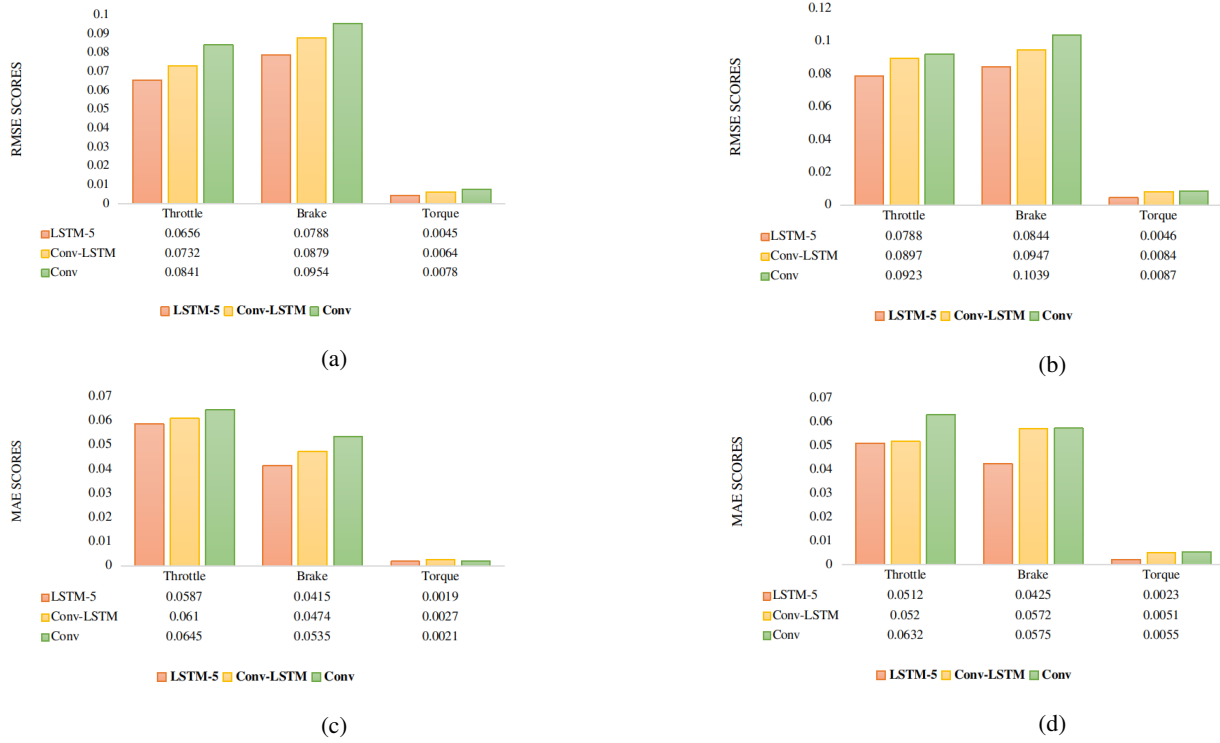


Fig. 8: Individual throttle, brake, and torque RMSE and MAE scores on human driving. (a),(c) RMSE and MAE scores of the throttle, brake, and torque for LSTM-5, Conv-LSTM, and Conv network using smooth-L1 loss function, respectively. (b)(d) RMSE scores of the throttle, brake, and torque for LSTM-5, Conv-LSTM, and Conv network, respectively, using mse loss function.

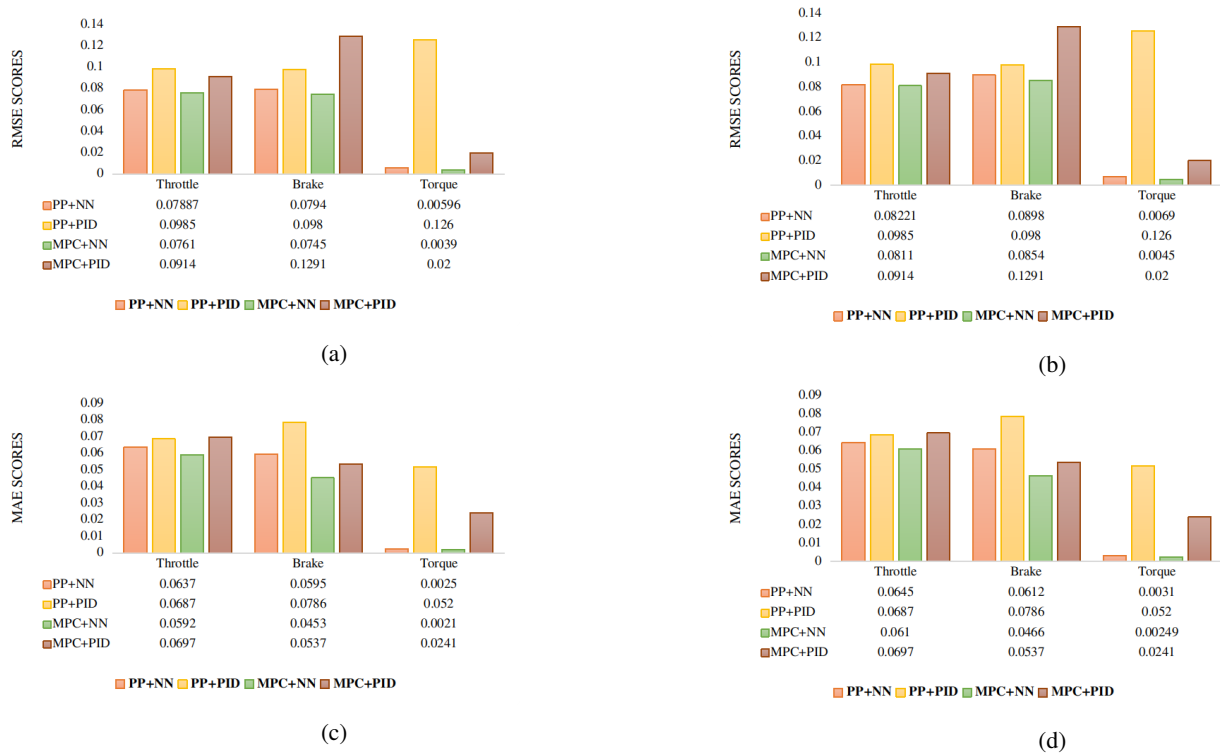


Fig. 9: Individual throttle, brake, and torque RMSE and MAE scores comparison between LSTM-5 (proposed method) and PID along with path tracking algorithms (PP and MPC). (a),(c) RMSE and MAE scores for smooth-L1 loss function. (b),(d) RMSE and MAE scores for the mse loss function.

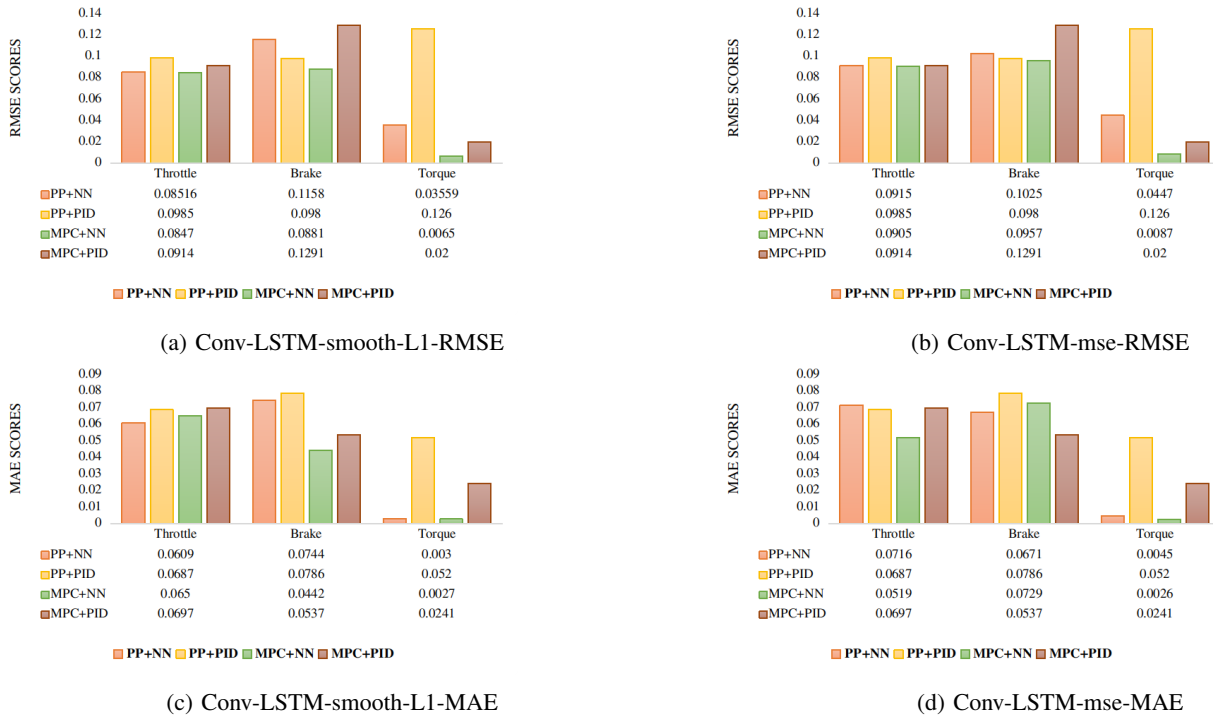


Fig. 10: Individual throttle, brake, and torque RMSE and MAE scores comparison between Conv-LSTM and PID along with path tracking algorithms (PP and MPC). (a),(c) RMSE and MAE scores for smooth-L1 loss function. (b),(d) RMSE and MAE scores for mse loss function.

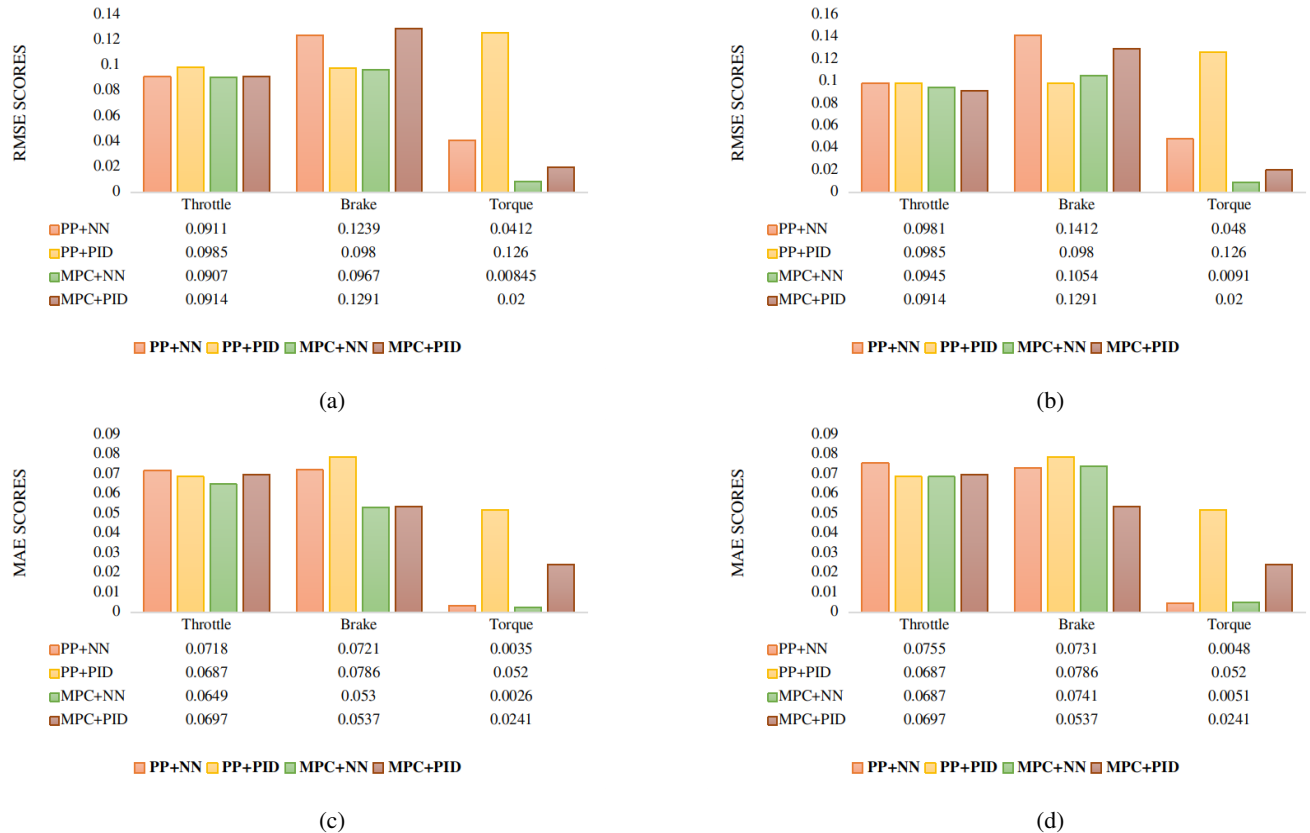


Fig. 11: Individual throttle, brake, and torque RMSE and MAE scores comparison between Conv-LSTM and PID along with path tracking algorithms (PP and MPC). (a),(c) RMSE and MAE scores for smooth-L1 loss function. (b),(d) RMSE and MAE scores for mse loss function.